„This is the peer reviewed version of the following article: Sebastian Henning, Laura Kühn, Juan Herranz, Maarten Nachtegaal, Alexander Eychmüller and Thomas J. Schmidt (2017). Effect of Acid Washing on Oxygen Reduction Reaction Activity of Pt-Cu Aerogel Catalysts. Electrochimica Acta, Volume 233, 10 April 2017, Pages 210-217, which has been published in final form at DOI:10.1016/j.electacta.2017.03.019.

Effect of Acid Washing on Oxygen Reduction Reaction Activity of Pt-Cu Aerogel Catalysts

Sebastian Henning[a,‡], *Laura Kühn*[b,‡], *Juan Herranz*[a,*], *Maarten Nachtegaal*[c], *Alexander Eychmüller*[b] *and Thomas J. Schmidt*[a,d]

[a]Electrochemistry Laboratory, Paul Scherrer Institut, 5232 Villigen, Switzerland

[b]Physical Chemistry, Technische Universität Dresden, Bergstr. 66b, 01062 Dresden, Germany

[c]Paul Scherrer Institut, 5232 Villigen, Switzerland

[d]Laboratory of Physical Chemistry, ETH Zurich, 8093 Zurich, Switzerland

* Corresponding author; E-mail: juan.herranz@psi.ch

‡These authors contributed equally

Keywords PEFC, ORR, Dealloying, Aerogels, X-ray absorption

Abstract

Developing highly active and durable oxygen reduction reaction (ORR) catalysts is crucial to reduce the cost of polymer electrolyte fuel cells (PEFCs). To meet those requirements, unsupported Pt-Cu alloy nanochains (aerogels) were synthesized by a simple co-reduction route in aqueous solution and their structure was characterized by X-ray absorption spectroscopy and STEM-EDX. These catalysts exceeded the ORR activity of commercial Pt/C catalysts by more than 100 % in RDE experiments and met the US DOE targets, thereby qualifying as very promising materials. The behavior of Pt-Cu aerogels under PEFC operation conditions was mimicked by acid washing experiments which showed that the Cu content in the alloy phase and ORR activity decrease through this step. Comparing composition, structure and ORR activity for various specimens, the Cu content in the alloy phase was identified as the main descriptor of ORR activity. An almost linear correlation was found between those two parameters and complemented by supporting data from the literature.

1. Introduction

Hydrogen powered polymer electrolyte fuel cells (PEFCs) are considered a viable energy source for all-electric vehicles [1]. In order to become more competitive with respect to alternative technologies, i.e. batteries, the system cost of PEFCs needs to be reduced. An important fraction of the overall costs is attributed to the use of expensive catalyst materials to accelerate the anodic hydrogen oxidation (HOR) and the cathodic oxygen reduction reaction (ORR) in the fuel cell [2]. Due to its slow kinetics, the latter ORR causes more than 50 % of the cell voltage losses during PEFC operation [3]. Thus, the development of O_2-reduction catalysts with enhanced activities that exceed state-of-the-art materials consisting of Pt nanoparticles supported on carbon [2] is of great importance. This improvement is typically achieved by alloying Pt with various transition

metals (e.g. Ni, Cu, Co) [4-7], thereby tuning (i.e., decreasing) the surface binding energies of adsorbed O-intermediates.

On top of these activity requirements, state-of-the-art Pt-based catalysts undergo significant losses of performance during PEFC operation due to the corrosion of their carbon support [8, 9]. As a result, research effort increasingly focuses on materials with C-free supports, or even fully unsupported catalysts [10-12]. Among the latter, aerogels consisting of tridimensionally interconnected metal nanoparticles provide the large electrochemical surface areas and porosities required for PEFC implementation, and can additionally be prepared in the bimetallic compositions required for an enhanced ORR activity [13, 14]. In this respect, our previous work on non-supported Pt-Ni aerogels [14] showed that these materials yield a Pt_3Ni alloy upon contact to acid, reaching the ORR activity target for automotive PEFCs set by the US Department of Energy (DOE) (i.e., 440 A/gPt at 0.9 V vs. the reversible hydrogen electrode (V_{RHE})). Looking for a further improvement, we have extended this approach to the preparation of Pt-Cu aerogels for which higher ORR activities can be excepted on the basis of the larger decrease of the oxygen binding energies on these alloy surfaces [15].

An important, yet often overlooked aspect for PEFC implementation of such Pt alloy catalysts is the leaching of their non-noble metal component, triggered by the acidic reaction environment concomitant to the perfluorosulfonic acid groups in the ionomer and membrane [16, 17]. Such exposure to acid can change the composition and corresponding catalytic properties of the Pt alloy catalyst. Additionally, the leached metal ions have a greater affinity for sulfonic acid groups than H^+, therefore poisoning the ionomer and negatively impacting PEFC performance [18, 19]. In some works dealing with Pt-Cu alloys with an initially large non-noble metal content (i.e. prone to severe Cu leaching), this effect was circumvented by acid washing the membrane

electrode assembly after Cu dissolution and prior to PEFC operation, as to restore the ionomer's initial H^+-inventory [20-22]. Thus, in this work we focus on two Pt-Cu aerogels with different initial copper contents, and mimic the dealloying effects related to MEA fabrication / PEFC operation by acid washing these materials. The relations established between the composition, structure and ORR activity of the resulting catalysts provide valuable insight on the key parameters that determine their reactivity.

2. Experimental

2.1 Synthesis

Pt-Cu hydrogels were prepared by a simple co-reduction route in aqueous solution under ambient conditions (room temperature, air). Briefly, Pt and Cu precursors were dissolved in water (18.2 MΩ·cm, Millipore) and reduced by $NaBH_4$. For the synthesis of Pt_3Cu hydrogel, 585µL of a 0.205 M H_2PtCl_6 solution (8 wt. % in H_2O, Sigma Aldrich) [final reactant concentration 0.15 mM] and 4 ml of a freshly prepared 10 mM $CuCl_2$ solution ($CuCl_2$*$2H_2O$ 99.999 %, Sigma Aldrich) [final reactant concentration 0.05 mM] were dissolved in 790 mL water and stirred until mixing was complete. Subsequently, 8.4 mL of freshly prepared 0.1 M $NaBH_4$ solution (granular, 99.99 %, Sigma Aldrich) [$c(Pt^{4+} + Cu^{2+}):c(NaBH_4)=1:1.5$] were added under vigorous stirring. In order to obtain PtCu hydrogel, 8 mL of a freshly prepared 10 mM K_2PtCl_4 solution (K_2PtCl_4 99.99 %, Sigma-Aldrich) [final reactant concentration 0.10 mM] and 8 ml of a 10 mM $CuCl_2$ solution [final reactant concentration 0.10 mM] were mixed in 780 mL water. 4.0 ml of freshly prepared 0.1 M $NaBH_4$ solution [$c(Pt^{4+} + Cu^{2+}):c(NaBH_4)=1:1.25$] were added to reduce the metal salts. Upon addition of $NaBH_4$, the color of the solutions turned immediately from light yellow to dark brown. The solutions were kept stirring for another 30 min. Afterwards, the reaction solutions were divided and transferred to 100 mL vials. After about four (PtCu) to six (Pt_3Cu) days, black hydrogel was formed at the bottom of the containers. The hydrogel parts

obtained from the same synthesis were collected in a small vial and washed with water. For this, half of the supernatant was removed and replaced cautiously with fresh water. This step was repeated six times. Afterwards, the solvent was exchanged stepwise with acetone. Again, half of the supernatant was removed and replaced by acetone. This step was repeated 11 times. The resulting anhydrous gels were transferred to a critical point dryer (Critical Point Dryer 13200J-AB, SPI Supplies) operating with CO_2.

2.2 XAS Spectroscopy

XAS spectra at the Pt L_3 and Cu K edges were recorded at the SuperXAS beamline of the Swiss Light Source (Paul Scherrer Institut, Villigen, Switzerland), whereby the beam current and the energy of the storage ring were 400 mA and 2.4 GeV, respectively. All EXAFS spectra at the Pt L_3 and Cu K edges were recorded in transmission mode using N_2-filled ionization chambers. A reference foil was measured simultaneously between the transmitted X-ray intensity and a third ionization chamber. The polychromatic beam was collimated by a Rh (at the Pt L_3 edge) or Si coated (at the Cu edge) collimating mirror. The mirror was followed by a channel-cut crystal Si (111) monochromator. Focusing of the beam to a spot of 100 x 100 micrometer was achieved by a toroidal mirror, located after the channel-cut monochromator. Measurements were performed ex-situ on pellets made of aerogel powder and cellulose in transmission mode. The quick-EXAFS (QEXAFS) method was used to increase time resolution [23]; 100 and 600 quick-XAS spectra were recorded at the Pt L_3 and Cu K edges, respectively. These XAS data were first analyzed with the JAQ analyzer software which allows averaging of individual XAS spectra into a single spectrum. Subsequently, Athena of the Demeter software package was used for normalization and background subtraction.[24] The energy units (eV) were then converted to photoelectron wave vector k units ($Å^{-1}$) by assigning the photoelectron energy origin, E_0, corresponding to $k = 0$, to the first inflection point of the absorption edge. The resulting $\chi(k)$ functions for the Pt

and Cu edge spectra were weighted with k^2 and then Fourier-transformed to obtain pseudo radial structure functions (RSFs). The fit of the EXAFS oscillations was performed with Artemis[24] using a face centered cubic Pt-Cu structure for the paths description. In case of the hetero-metallic pairs (Pt-Cu and Cu-Pt) in the nearest neighboring of the adsorbing atoms, atoms of one type were substituted with atoms of the opposite type. Amplitude reduction terms were calculated from EXAFS fits of Pt and Cu reference foils assuming a coordination number of 12 and amounted to $S_{0,Cu}^2 = 0.87$ and $S_{0,Pt}^2 = 0.81$, respectively.

2.3. Electrochemical measurements

Electrolyte solutions were prepared from 60% $HClO_4$ (Kanto Chemical Co., Inc.) diluted in ultrapure water (18.2 MΩ cm, Elga Purelab Ultra). High purity N_2 (5.0), O_2 (5.0) and CO (4.7) were purchased from Messer AG, Switzerland. The benchmark catalyst for this study is a Pt/Vulcan XC-72 electrocatalyst with a Pt weight fraction of 30 % (E-TEK Inc., Lot# C0160311). The electrochemical setup used has been described in detail in a previous work [14]; in brief it consists of a three electrode glass cell, equipped with a gold mesh counter electrode, reversible hydrogen reference electrode and PTFE-made rotating-ring disk electrode (RRDE, Pine Research Instrumentation) as working electrode. Thin-film electrodes were prepared by dispersing catalyst materials in mixtures of ultrapure water (18.2 MΩ cm, Elga Purelab Ultra) and isopropanol (99.9 %, Chromasolv Plus® for HPLC, Sigma Aldrich), followed by 10 min sonication in an ultrasonic bath (USC100T, 45 kHz, VWR). Fractions of the inks were pipetted onto the glassy carbon inset of the RRDE to obtain catalyst loadings of 15 $\mu g_{Pt}/cm^2_{electrode}$. Subsequently, coatings were dried under a gentle N_2-flux.

3. Results and Discussion

Pt-Cu aerogels with two different metal precursor ratios were synthesized by co-reduction as specified in section 2.2.1, and ICP-OES analysis of the products yielded the expected Pt:Cu atomic ratios of 3:1 and 1:1, respectively; the samples will therefore be denoted Pt_3Cu and PtCu in the following.

In parallel, fractions of Pt_3Cu and PtCu hydrogels (cf. section 2.2.1) were suspended in 0.1 M $HClO_4$ solution for 2 days before the acetone exchange and final supercritical drying step. The resulting acid washed materials (Pt_3Cu AW and PtCu AW) showed lower Cu contents than their as-synthesized counterparts, namely 20 and 26 at. % for Pt_3Cu AW and PtCu AW, respectively (as opposed to 25 and 50 at. % for Pt_3Cu and PtCu; see Table 2).

Fig 1 shows representative transmission electron microscopy (TEM) images for Pt_3Cu, PtCu and their acid washed derivatives that all exhibit the typical 3D nanochain structure observed in previous works on similar materials [13, 14]. Size distributions were determined by measuring the nanochain diameter at different positions along the chains and amounted to 3.8 ± 1.0, 3.9 ± 1.1, 4.0 ± 1.0 and 3.7 ± 0.9 nm for Pt_3Cu, Pt_3Cu AW, PtCu and PtCu AW, respectively (see Fig SI-1 for TEM images at higher resolution). Besides the nanochain network, large needle-like structures can be observed in the PtCu sample (Fig 1C) which are attributed to the presence of copper oxide that precipitates during the synthesis. This hypothesis is supported by XPS spectra at Cu 2p binding energies (see Fig SI-2), in which the peaks at ~ 962 eV and ~ 942 eV in the PtCu spectrum indicate the presence of copper oxides [25]. For the same specimen after acid washing, PtCu AW, those needle-like structures could not be observed anymore when TEM images were taken at different locations (not shown here) in agreement with the disappearance of Cu oxides features in the XPS spectrum (cf. Fig. SI-2D). As for Pt_3Cu, no effect of the acid washing on its morphology and composition was discernible from TEM and XPS.

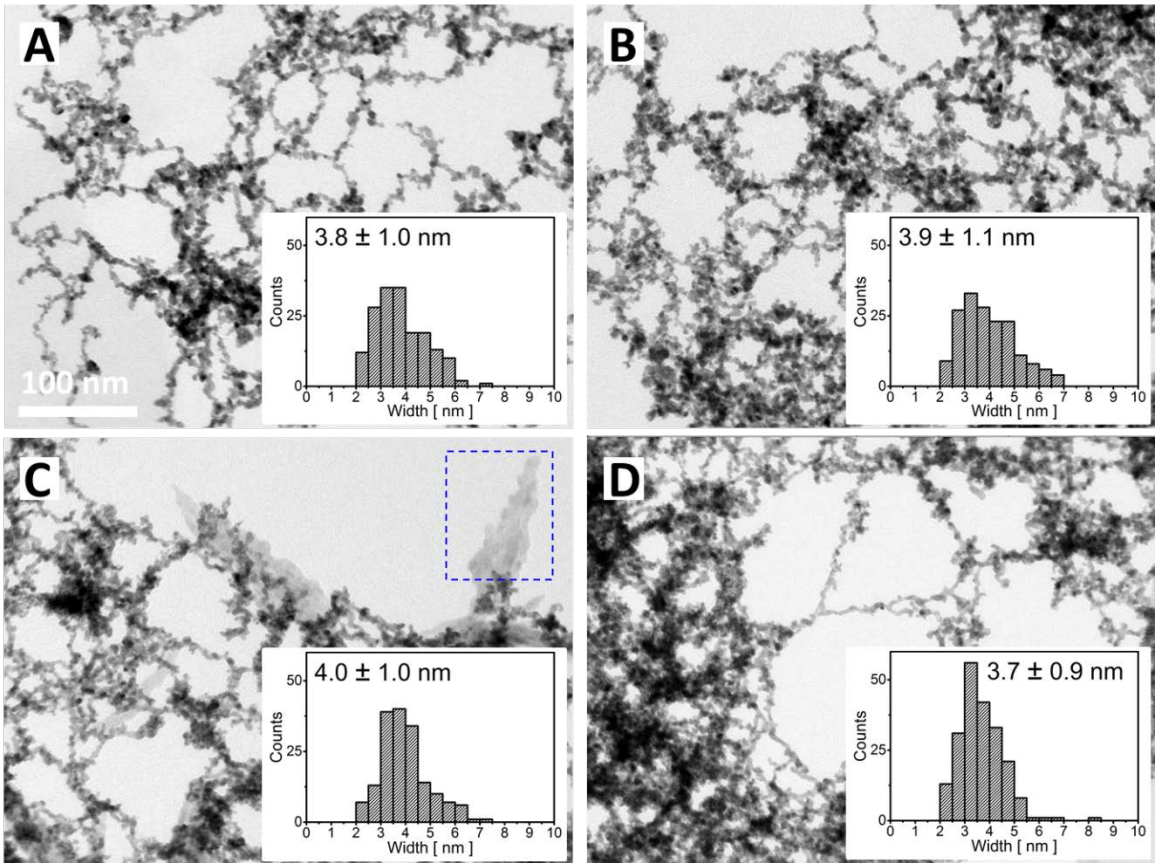

Figure 1. TEM images of Pt_3Cu (A: as synthesized, B: acid washed) and PtCu (C: as synthesized, D: acid washed) aerogels; the insets show the corresponding distributions of nanochain diameters and the copper oxide side phase for PtCu (C) is highlighted by a blue frame.

Next, the ORR activity of the as-synthesized and acid washed Pt-Cu aerogels was determined using rotating disk electrode (RDE) voltammetry [26] in 0.1 M $HClO_4$ electrolyte. The mass-specific ORR activities at 0.95 V_{RHE} in Fig. 2A were extracted from anodic sweeps at 5 mVs^{-1} and 1600 rpm in O_2-satured electrolyte after correcting for cell resistance and mass transport limitations applying the Koutecky-Levich equation [3]. Both Pt_3Cu and PtCu show

≈ 1.5-2 fold higher mass-specific ORR activities than the benchmark Pt/C catalyst, whereby the latter aerogel (PtCu) exceeds by ≈ 30 % the DOE ORR activity target for 2017, extrapolated from the reported value [1] of 440 A/g_{Pt} at 0.9 V_{RHE} to the 0.95 V_{RHE} used herein by assuming a Tafel slope of 60 mV dec^{-1} [27]. Interestingly, mass-specific ORR activities were lower for Pt_3Cu AW (- 10 % vs. Pt_3Cu) and PtCu AW (- 25 % vs. PtCu), indicating that the loss of copper upon exposure to acid is detrimental to the aerogels' catalytic activity. A similar trend was observed for surface-specific activities (cf. Fig. 2B) that were calculated by normalizing ORR currents with an average electrochemical surface area (ECSA) obtained from hydrogen underpotential deposition (H_{upd}) [17] and CO stripping charges (assuming conversion factors of 210 and 420 $\mu C/cm^2_{Pt}$, respectively) [28, 29] (cf. Fig. SI-3). The corresponding ECSAs used for normalization differed by less than 5 % among techniques (i.e., H_{upd} vs. CO-stripping), and are written vertically across the bars in Fig. 2B. Additionally, these values did not change significantly upon acid wasting, therefore excluding the formation of distinct Pt-skeleton core−shell structures that would lead to an increase in ECSA following Cu-dealloying [6, 7, 30-32]. As discussed in a previous work [14], the ≈ 3-fold increase of ECSA-specific activity for Pt-Cu aerogels vs. Pt/C is mainly related a weaker adsorption of O-intermediates, in terms caused by a downshift of the d-band center [33] (electronic effect) induced by the alloying with Cu [15].

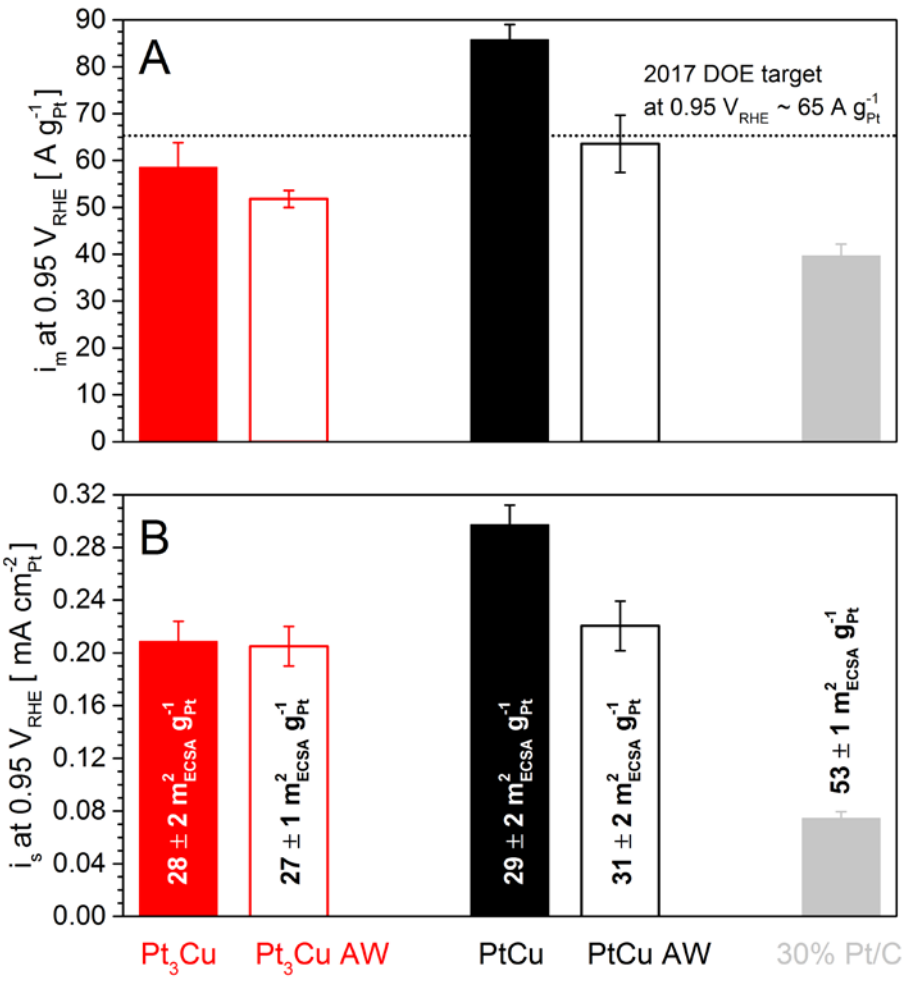

Figure 2. Mass-specific (A) and Pt-ECSA specific (B) ORR activity values at 0.95 V_{RHE} for Pt-Cu aerogels as synthesized (solid) and acid washed (hollow), plus a 30 % Pt/C benchmark (averaged from 3 independent measurements). The dotted line represents the DOE ORR activity target at 0.95 V_{RHE}, extrapolated from the benchmark value of 440 A/g_{Pt} at 0.9 V_{RHE} [1] assuming a Tafel slope of 60 mV dec^{-1} [27]. Vertical column labels are ECSA values averaged from H_{upd} and CO stripping charges.

Since the decrease of ORR activity observed for the Pt-Cu aerogels upon acid washing is expected to be reproduced during MEA preparation / PEFC operation, it is fundamental to

unravel the reasons for this behavior in order to assess the material's PEFC applicability. Comparing the ORR activity for all four specimens, the trend PtCu > PtCu AW ≥ Pt_3Cu ≥ Pt_3Cu AW qualitatively matches the Cu content in the as-synthesized and acid-washed aerogels, determined by ICP-OES, thus agreeing with reports by the Strasser group correlating ORR activity and Cu concentration [22, 34]. However, those studies included catalysts with copper contents ≥ 50 at. % that experienced significant Cu leaching during the initial voltammetric conditioning step [34]. Analogously, considering the existence of a copper oxide side phase in PtCu, the initial Cu content (derived by ICP-OES) in these aerogel catalysts can be a misleading property to relate to their ORR activity.

With this motivation, these four samples were investigated by X-ray diffraction (XRD) to determine their degree of alloying and corresponding composition. As discernible from the inset in Fig. 3, the (111) reflection peak for PtCu is at larger 2θ values than for Pt_3Cu indicating higher Cu content in the alloy phase and coinciding with the ~ 50 % greater surface-specific ORR activity. Additionally, the small reflection peak at ~ 35° for the PtCu spectrum can be assigned to the copper oxide side phase that was also observed on the TEM images (cf. Fig 1) and the XPS spectrum (cf. Fig SI-2). Furthermore, upon acid washing (i.e. sample PtCu AW) the (111) reflection peak shifts to lower angles and almost coincides with the peaks of Pt_3Cu and Pt_3Cu AW, thereby indicating Cu loss from the alloy phase. This in turn can explain the significant decrease in ORR activity for PtCu upon acid washing and similar activities for PtCu AW, Pt_3Cu and Pt_3Cu AW. In parallel, the reflection peak corresponding to copper oxide disappears in the PtCu AW spectrum, in agreement with observations from both TEM and XPS. Applying Vegard's law [35] the stoichiometric compositions were determined as $Pt_{65}Cu_{35}$ (PtCu), $Pt_{71}Cu_{29}$ (PtCu AW), $Pt_{75}Cu_{25}$ (Pt_3Cu) and $Pt_{76}Cu_{24}$ (Pt_3Cu AW); besides for PtCu,

containing a copper oxide side phase, these figures are similar to the initial ICP-OES values (cf. Table 2).

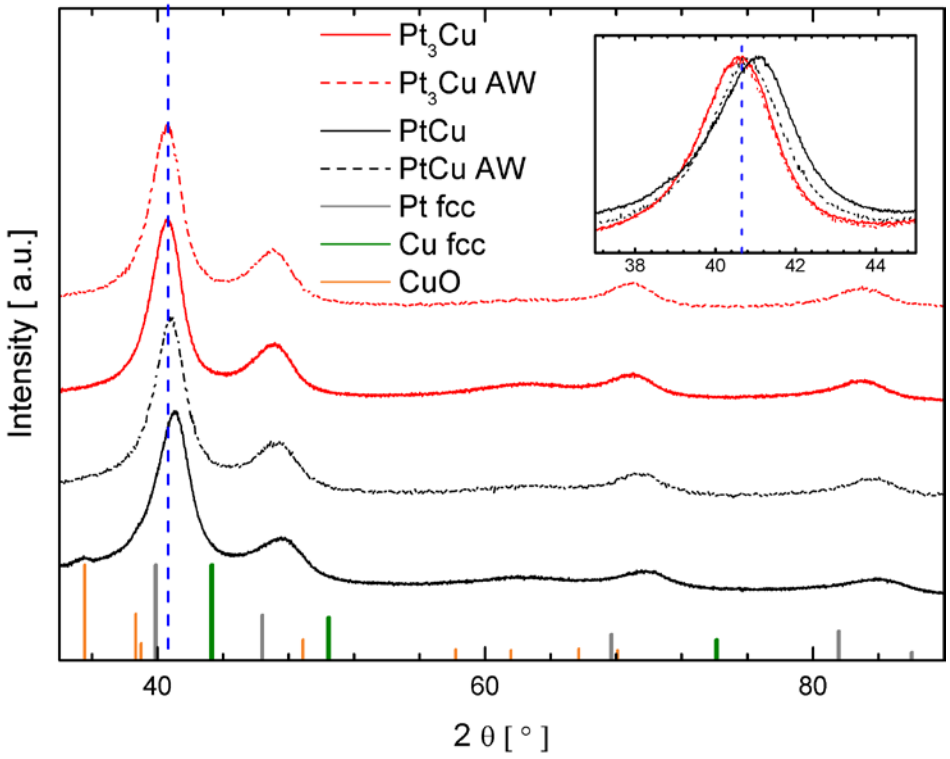

Figure 3. XRD spectra for Pt_3Cu (solid red), PtCu (solid black) and respective acid washed samples (dotted). Reflections for metallic Pt [36], Cu [37] and CuO [38] are shown as a reference bars at the bottom of the chart; the inset shows a magnification of the (111) reflections.

Next, the aerogels' structure was studied further to potentially unravel additional reasons for the apparent relation between ORR activity and Cu content. First, extended X-ray absorption spectrum fine structure spectroscopy (EXAFS) was performed at the Pt L_3 (11564 eV) and Cu K (8979 eV) edges to get insight into the local structure of the Pt-Cu aerogels. Figure SI-4 displays the Fourier transformed (FT) EXAFS spectra at the Cu K edge in R-space for all samples; resembling spectra are observed with the only exception of the PtCu aerogel, which features a peak at ≈ 1.5 Å that can be assigned to Cu-O scattering contributions from the copper oxide side-

phase observed in TEM images and XPS spectra (cf. Fig. 1 and Fig. SI-2). As expected, those contributions disappear for PtCu AW suggesting that the sidephase is removed upon acid washing, which is consistent with the corresponding TEM and XPS results (cf. Fig 1 and Fig SI-2).

As a result of the compositional heterogeneity caused by the presence of a Cu oxide phase, the fitting of the first shell EXAFS for PtCu was not successful. For all three other samples, the result of the simultaneous first shell fit at both edges is summarized in Table 1 and the Fourier transformed EXAFS spectra and corresponding fits are shown in Figure SI-5. As summarized in Table 1, coordination numbers and bond lengths (CNs, Rs) for Pt_3Cu and Pt_3Cu AW are similar, in agreement with their alike XRD profiles and ORR activities. What is more, almost identical CN- and R-values have been reported previously for carbon-supported Pt_3Cu nanoparticles with a comparable particle size [39], endorsing the observation from TEM images that the aerogels consist of individual nanoparticles connected to nanochains. Additionally, on the basis of the coordination numbers in Table 1, the local bimetallic composition x_{Pt} and x_{cu} was determined as follows and is summarized in Table 2 [40, 41].

$$\frac{x_{Pt}}{x_{Cu}} = \frac{CN_{Cu-Pt}}{CN_{Pt-Cu}} \qquad [1]$$

For both samples, there is a close agreement between the molar ratios inferred from EXAFS and XRD, thus providing another indication that Pt_3Cu and Pt_3Cu AW are homogeneous bimetallic alloys at all spatial scales [41]. A more quantitative descriptor of the local homogeneity (up to ~ 6 Å) of bimetallic nanoparticles is the Cowley short range order parameter (α), given by [40, 42]:

$$\alpha = 1 - \frac{CN_{Pt-Cu}/(CN_{Pt-Pt} + CN_{Pt-Cu})}{x_{Cu}} \qquad [2]$$

whereby $CN_{Pt\text{-}Cu}$ and $CN_{Pt\text{-}Pt}$ refer to number of nearest Cu and Pt neighbours surrounding Pt atoms, respectively, and x_{Cu} is derived from Equation 1 [41]. This calculation yields values of ~ 0 for both samples, which is again indicative of a homogeneously random alloy [40] and similar to the results for Pt-Ni aerogels that were investigated in a previous study [14].

Table 1. Coordination number (CN), atomic bond length (R), mean squared bond length disorder (σ^2), and shift of energy (ΔE_0) derived from the simultaneous fitting of the EXAFS (Pt L_3 and Cu K edges) for Pt_3Cu, Pt_3Cu AW and PtCu AW aerogels, along with the corresponding R factors (fit quality parameter [43], whereby R-values ≤ 0.02 are regarded as indicative of high quality fits).

Aerogel	Bond	CN	R [Å]	σ^2 [10^{-3} Å^2]	ΔE_0 [eV]	R-factor
Pt_3Cu	Pt-Pt	7.8 ± 0.7	2.71 ± 0.004	7 ± 1	4.8 ± 0.6	0.015
	Pt-Cu	2.6 ± 0.6	2.67 ± 0.016	11 ± 2	8.4 ± 2.4	
	Cu-Pt	7.6 ± 1.3	2.67 ± 0.016	11 ± 2	2.5 ± 0.9	
	Cu-Cu	2.9 ± 1.3	2.65 ± 0.041	10 ± 5	6.4 ± 4.3	
Pt_3Cu AW	Pt-Pt	7.8 ± 0.8	2.71 ± 0.004	7 ± 1	4.8 ± 0.8	0.017
	Pt-Cu	2.3 ± 0.8	2.68 ± 0.028	12 ± 3	9.2 ± 3.6	
	Cu-Pt	7.8 ± 2.6	2.68 ± 0.028	12 ± 3	2.3 ± 2.2	
	Cu-Cu	2.6 ± 2.3	2.65 ± 0.067	9 ± 8	4.9 ± 8.1	
PtCu AW	Pt-Pt	7.2 ± 1.0	2.69 ± 0.006	7 ± 1	3.1 ± 1.0	0.026
	Pt-Cu	3.4 ± 1.1	2.67 ± 0.030	14 ± 3	8.0 ± 3.7	
	Cu-Pt	8.2 ± 2.2	2.67 ± 0.030	14 ± 3	2.2 ± 2.0	
	Cu-Cu	2.4 ± 1.5	2.64 ± 0.049	9 ± 6	6.4 ± 6.7	

On the other hand, the EXAFS fit for PtCu AW yielded an R-factor that was slightly larger than 0.02, indicating a lower quality fit [43]. In this case the local bimetallic composition deviated only slightly from the ICP-OES result (x_{Cu} ~ 26 at. % for the latter, vs. 29 at. % from EXAFS) and Cowley's short range order parameter amounted to ~ -0.1. Sufficient accuracy of the EXAFS fit provided, these results point towards a homogeneous alloy [40] with a shorter Pt-Pt bond length than the Pt_3Cu samples (2.69 vs. 2.71 Å) that may explain the slightly higher ORR activity of PtCu AW. Indeed, this documented impact of the Pt-Pt bond length on the ORR activity [39, 44], whereby alloy-induced compressive lattice strain leads to a weaker adsorption of O-intermediates [45], is typically referred to as a 'geometric effect', in contrast to the 'electronic effect' mentioned earlier. While the discussion about the relative contribution of geometric and electronic effects to the ORR activity is ongoing, Kaito et al. [39] have presented a linear correlation between Pt-Pt bond length and ORR activity for alloys of Pt with other transition metals (i.e., Ni, Co, Cu) in which shorter bond lengths are directly related with a higher ORR activity, which is in line with our own trend (PtCu AW > Pt_3Cu ≥ Pt_3Cu AW).

Table 2. Chemical compositions (at. %) obtained from ICP-OES, XRD, EDX and EXAFS data and Cowley short range order parameter for various aerogel samples.

Aerogel	x_{Cu} (ICP-OES)	x_{Cu} (XRD)	x_{Cu} (EDX)	x_{Cu} (EXAFS)	α (Pt-Cu)	α (Cu-Pt)
Pt_3Cu	25	25 ± 3	22 ± 7	0.24 ± 0.08	+0.03	+0.05
Pt_3Cu AW	20	24 ± 1	20 ± 5	0.23 ± 0.12	-0.01	+0.03
PtCu	50	35 ± 5	39 ± 2	n/a	n/a	n/a
PtCu AW	26	29 ± 4	29 ± 3	0.29 ± 0.11	-0.14	-0.09

In a last step, scanning transmission electron microscopy in combination with energy dispersive X-ray spectroscopy (STEM-EDX) was used to investigate the alloy homogeneity and structure (e.g. formation of core shell structures [46]) for selected areas, in contrast to the bulk techniques discussed above (XRD and XAS). Representative STEM-EDX images for all four specimens are shown in Figure 4, and their respective compositions calculated by averaging Cu and Pt counts from EDX maps over at least ten regions (~ 150 nm^2 each) are summarized in Table 2. Visually comparing the separate EDX maps for Pt and Cu atoms (not shown here) for all four specimens, no inhomogeneities can be observed. For Pt_3Cu and Pt_3Cu AW (Fig 4A and 4B), however, we sporadically found regions with Cu contents of up to ~ 30 at. % upon quantitative analysis of EDX maps, which explain the rather large error bars in Table 2. Nonetheless, in sight of the Cowley short range order parameters of ~ 0 derived from bulk-sensitive EXAFS (cf. Table 2), these regions are not representative of the overall samples' homogeneity. Moreover, at the investigated magnification, no indication was found for the formation of a core shell type structure after acid washing, i.e., a Cu deficient shell and a Pt rich core.

Similarly to the Pt_3Cu specimens, PtCu (Fig. 4C) shows a homogeneous distribution of Pt and Cu atoms in the EDX map, whereby the average x_{Cu} was determined to be 0.39; this is slightly lower than the value 0.5 derived from ICP-OES, probably due to the presence of Cu oxides in parts of the sample, while remaining in good agreement with XRD data (cf. Table 2). After acid washing (Fig. 4D) the homogeneity of PtCu AW is retained but x_{Cu} decreases to 0.29, again in good agreement with values from ICP-OES, XRD and EXAFS.

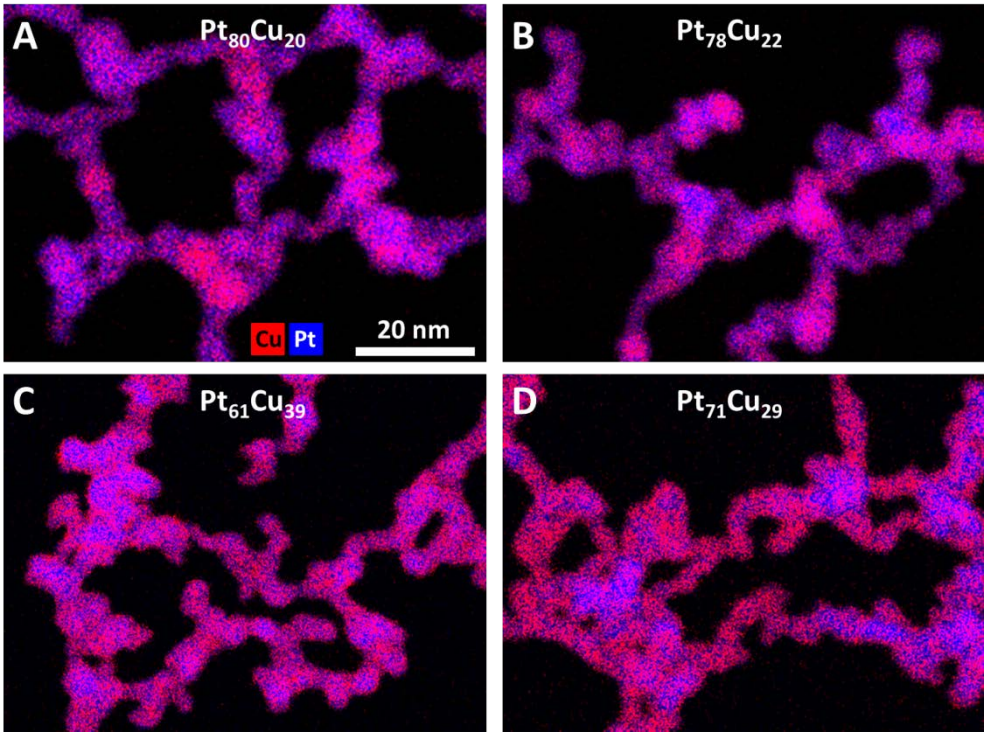

Figure 4. STEM-EDX images of Pt_3Cu (A: as synthesized, B: acid washed) and PtCu (C: as synthesized, D: acid washed) aerogels; Cu and Pt atoms are displayed in red and blue, respectively and stoichiometric compositions are included at the top of the images.

Based on the combined findings from XRD, STEM-EDX and EXAFS, the main reason for the difference in ORR activities for the investigated samples appears to be the Cu content in the Pt-Cu alloy phase. Thus, in Figure 5 the ORR surface-specific activities were plotted vs. the initial alloy phase Cu contents derived through Vegard's law on the basis of the XRD data (cf. Table 2). To extend this analysis to a wider range of Cu contents, we included in Figure 5 ORR activity values reported for several Pt-Cu/C catalysts (cf. references [30, 34, 35, 39, 47, 48]), adapted from the customary value of 0.9 V_{RHE} to the 0.95 V_{RHE} used herein by assuming a Tafel slope of 60 mV dec^{-1}. Those references were selected carefully following three criteria to increase

comparability. First, the ORR activities were recorded under similar conditions [49], i.e., in O_2-saturated 0.1 M $HClO_4$ and using scan rates between 5 and 10 mVs^{-1}. Second, the alloy compositions were determined by either XRD or EDX (which in our case yielded similar results, cf. Table 2) and, for alloys with an initially high Cu-content, they were assessed after voltammetric conditioning. And third, only materials with ECSAs below 50 m^2/g_{Pt} were considered to minimize the influence of the particle size effects on the ORR activity [17].

Interestingly, when the Cu range covered by the as-synthesized and acid washed aerogels in this work is considered (24 – 35 at. %), an almost linear correlation between ORR activity and alloy phase Cu content can be found. When considering additional values from the literature, this correlation still holds true for the majority of data points, as illustrated by a grey dashed line in Fig. 5. The deviation of some results from the general trend can be explained by the fact that the corresponding Pt-Cu/C catalysts were prepared from Cu rich alloys (≥ 50 at. % Cu) that were either electrochemically dealloyed or acid washed before composition and ORR activity were determined. Considering the differences in starting materials and preparation methods, as well as potential non-uniformity of the samples and unreliability in the determination of their composition, the alloy phase Cu content appears to be the critical parameter determining catalytic activity for this sort of materials. The observed correlation can in terms be explained by the d-band center theory, since an increase in the Cu content leads to a downshift of the d-band center, thereby increasing the number of free sites for O_2 adsorption and thus leading to the observed enhancement of the ORR activity [33].

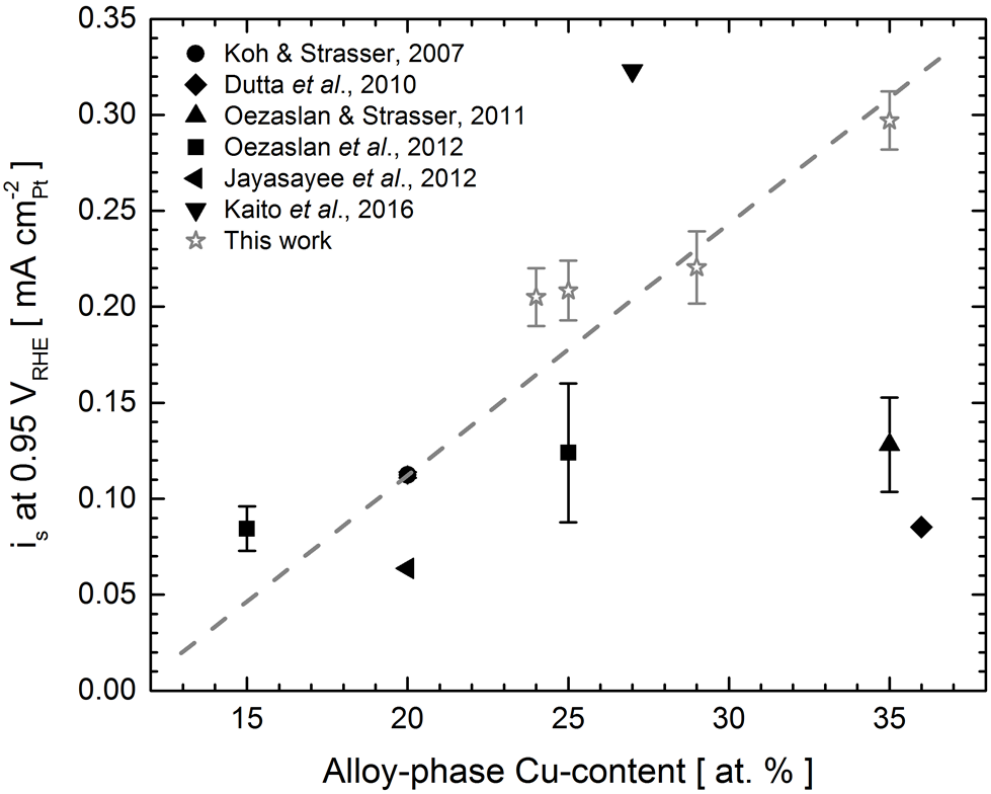

Figure 5. Surface-specific ORR activities at 0.95 V_{RHE} (from Fig. 2 or various literature sources) vs. Cu content in the alloy phase (from XRD or EDX). The activity values for Pt-Cu/C catalysts (black symbols) are deduced from references [30, 34, 35, 39, 47, 48], assuming a Tafel slope of 60 mV dec^{-1} and the grey dashed line serves as guide for the eye of the linear correlation.

4. Conclusion

In summary, we have presented the synthesis of bimetallic Pt-Cu aerogels with different Cu contents and studied the effect of acid washing (a mimic of the low pH in the PEFC) on the composition, structure and catalytic activity of these materials. The as-synthesized samples consist of Pt-Cu alloys, along with a copper oxide side phase for the aerogel with a higher Cu content. Upon acid washing, this oxide was removed and the Cu content in the alloy phase

decreased but the overall aerogel structure was not altered. Additionally, as-synthesized Pt-Cu aerogels were tested for ORR activity in RDE experiments, whereby they met or even exceeded the US DOE ORR mass-specific activity target by up to 30 %. Acid washed specimens showed lower ORR activity which could be related to the reduced Cu content in the alloy phase which, in agreement with previous reports in the literature, is linearly related to the ORR activity due to the upshift of the d-band center induced by a decrease of the alloy Cu content. Most importantly, since the loss of copper upon acid washing reported here will likely be reproduced during PEFC operation, affecting catalyst activity and cell performance, aerogels should be submitted to resembling acid-washing or equivalent voltammetric conditioning steps (seemingly detrimental to their reactivity) prior to MEA implementation. Thus, in order to retain the outstanding initial ORR activity of the PtCu aerogel, future work will focus on minimizing Cu leaching for these materials.

5. Acknowledgement

The authors thank the Swiss Light Source for providing beamtime at the SuperXAS beamline. This work was funded by the Swiss National Science Foundation (20001E_151122/1), the German Research Foundation (EY 16/18-1) and the European Research Council (ERC AdG 2013 AEROCAT).

References

[1] O. Gröger, H.A. Gasteiger, J.P. Suchsland, J. Electrochem. Soc. 162 (2015) A2605-A2622.
[2] A. Kongkanand, M.F. Mathias, J. Phys. Chem. Lett. 7 (2016) 1127-1137.
[3] W. Sheng, H.A. Gasteiger, Y. Shao-Horn, J. Electrochem. Soc. 157 (2010) B1529.
[4] C. Wang, M. Chi, D. Li, D. Strmcnik, D. van der Vliet, G. Wang, V. Komanicky, K.C. Chang, A.P. Paulikas, D. Tripkovic, J. Pearson, K.L. More, N.M. Markovic, V.R. Stamenkovic, J. Am. Chem. Soc. 133 (2011) 14396-14403.
[5] P. Strasser, Rev. Chem. Eng. 25 (2009) 255-295.
[6] F. Hasché, M. Oezaslan, P. Strasser, ChemCatChem 3 (2011) 1805-1813.
[7] F. Hasché, M. Oezaslan, P. Strasser, J. Electrochem. Soc. 159 (2011) B24-B33.
[8] X.-Z. Yuan, H. Li, S. Zhang, J. Martin, H. Wang, J. Pow. Sourc. 196 (2011) 9107-9116.
[9] P.J. Ferreira, G.J. la O', Y. Shao-Horn, D. Morgan, R. Makharia, S. Kocha, H.A. Gasteiger, J. Electrochem. Soc. 152 (2005) A2256.
[10] A. Rabis, P. Rodriguez, T.J. Schmidt, ACS Catal. 2 (2012) 864-890.
[11] A. Patru, A. Rabis, S.E. Temmel, R. Kotz, T.J. Schmidt, Catal. Today 262 (2016) 161-169.
[12] E. Fabbri, A. Rabis, R. Kotz, T.J. Schmidt, Phys. Chem. Chem. Phys. 16 (2014) 13672-13681.
[13] W. Liu, P. Rodriguez, L. Borchardt, A. Foelske, J. Yuan, A.K. Herrmann, D. Geiger, Z. Zheng, S. Kaskel, N. Gaponik, R. Kotz, T.J. Schmidt, A. Eychmuller, Angew. Chem. Int. Ed. 52 (2013) 9849-9852.
[14] S. Henning, L. Kühn, J. Herranz, J. Durst, T. Binninger, M. Nachtegaal, M. Werheid, W. Liu, M. Adam, S. Kaskel, A. Eychmüller, T.J. Schmidt, J. Electrochem. Soc. 163 (2016) F998-F1003.
[15] J. Greeley, I.E.L. Stephens, A.S. Bondarenko, T.P. Johansson, H.A. Hansen, T.F. Jaramillo, RossmeislJ, ChorkendorffI, J.K. Nørskov, Nat. Chem. 1 (2009) 552-556.
[16] M. Pourbaix, Atlas of electrochemical equilibria in aqueous solutions, Pergamon Press, Oxford, 1966.
[17] H.A. Gasteiger, S.S. Kocha, B. Sompalli, F.T. Wagner, Appl. Catal. B: Environ. 56 (2005) 9-35.
[18] T. Okada, Effect of ionic contaminants, Handbook of Fuel Cells, John Wiley & Sons, Ltd 2010.
[19] T.A. Greszler, T.E. Moylan, H.A. Gasteiger, Modeling the impact of cation contamination in a polymer electrolyte membrane fuel cell, Handbook of Fuel Cells, John Wiley & Sons, Ltd 2010.
[20] L. Dubau, M. Lopez-Haro, J. Durst, L. Guétaz, P. Bayle-Guillemaud, M. Chatenet, F. Maillard, J. Mater. Chem. A 2 (2014) 18497-18507.
[21] B.H. Han, C.E. Carlton, A. Kongkanand, R.S. Kukreja, B.R. Theobald, L. Gan, R. O'Malley, P. Strasser, F.T. Wagner, Y. Shao-Horn, Energ. Environ. Sci. 8 (2015) 258-266.
[22] P. Mani, R. Srivastava, P. Strasser, J. Am. Chem. Soc. 112 (2008) 2770-2778.
[23] O. Müller, M. Nachtegaal, J. Just, D. Lützenkirchen-Hecht, R. Frahm, J. Synchrotron Rad. 23 (2016) 260-266.
[24] B. Ravel, M. Newville, J. Synchrotron Rad. 12 (2005) 537-541.
[25] C.D. Wagner, G.E. Muilenberg, Handbook of x-ray photoelectron spectroscopy : a reference book of standard data for use in x-ray photoelectron spectroscopy, Physical Electronics Division, Perkin-Elmer Corp., Eden Prairie, Minn., 1979.
[26] T.J. Schmidt, H.A. Gasteiger, G.D. Stäb, P.M. Urban, D.M. Kolb, R.J. Behm, J. Electrochem. Soc. 145 (1998) 2354-2358.

[27] U.A. Paulus, T.J. Schmidt, H.A. Gasteiger, R.J. Behm, J. Electroanal. Chem. 495 (2001) 134-145.
[28] K.J.J. Mayrhofer, D. Strmcnik, B.B. Blizanac, V. Stamenkovic, M. Arenz, N.M. Markovic, Electrochim. Acta 53 (2008) 3181-3188.
[29] F. Maillard, M. Eikerling, O.V. Cherstiouk, S. Schreier, E. Savinova, U. Stimming, Faraday Discuss. 125 (2004) 357-377.
[30] I. Dutta, M.K. Carpenter, M.P. Balogh, J.M. Ziegelbauer, T.E. Moylan, M.H. Atwan, N.P. Irish, J. Phys. Chem. C 114 (2010) 16309-16320.
[31] R. Yang, J. Leisch, P. Strasser, M.F. Toney, Chem. Mater. 22 (2010) 4712-4720.
[32] J. Erlebacher, M.J. Aziz, A. Karma, N. Dimitrov, K. Sieradzki, Nature 410 (2001) 450-453.
[33] V.R. Stamenkovic, B.S. Mun, M. Arenz, K.J. Mayrhofer, C.A. Lucas, G. Wang, P.N. Ross, N.M. Markovic, Nat. Mater. 6 (2007) 241-247.
[34] M. Oezaslan, F. Hasché, P. Strasser, J. Electrochem. Soc. 159 (2012) B444-B454.
[35] M. Oezaslan, P. Strasser, J. Pow. Sourc. 196 (2011) 5240-5249.
[36] T. Barth, G. Linde, Zeitschrift für Physikalische Chemie 121 (1926) 78-102.
[37] H.M. Otte, J. Appl. Phys. 32 (1961) 1536.
[38] O. García-Martínez, R.M. Rojas, E. Vila, J.L.M. de Vidales, Solid State Ionics 63 (1993) 442-449.
[39] T. Kaito, H. Tanaka, H. Mitsumoto, S. Sugawara, K. Shinohara, H. Ariga, H. Uehara, S. Takakusagi, K. Asakura, J. Phys. Chem. C 120 (2016) 11519-11527.
[40] A.I. Frenkel, Q. Wang, S.I. Sanchez, M.W. Small, R.G. Nuzzo, J. Chem. Phys. 138 (2013) 064202.
[41] M. Oezaslan, W. Liu, M. Nachtegaal, A.I. Frenkel, B. Rutkowski, M. Werheid, A.K. Herrmann, C. Laugier-Bonnaud, H.C. Yilmaz, N. Gaponik, A. Czyrska-Filemonowicz, A. Eychmuller, T.J. Schmidt, Phys. Chem. Chem. Phys. 18 (2016) 20640-20650.
[42] A.I. Frenkel, A. Yevick, C. Cooper, R. Vasic, Annu. Rev. Anal. Chem. 4 (2011) 23-39.
[43] http://bruceravel.github.io/demeter/artug/fit/happiness.html (accessed 24.11.2016).
[44] S. Mukerjee, S. Srinivasan, M.P. Soriaga, J. Mcbreen, J. Electrochem. Soc. 142 (1995) 1409-1422.
[45] P. Strasser, S. Koh, T. Anniyev, J. Greeley, K. More, C. Yu, Z. Liu, S. Kaya, D. Nordlund, H. Ogasawara, M.F. Toney, A. Nilsson, Nat. Chem. 2 (2010) 454-460.
[46] M. Oezaslan, F. Hasché, P. Strasser, J. Am. Chem. Soc. 4 (2013) 3273-3291.
[47] S. Koh, P. Strasser, J. Am. Chem. Soc. 129 (2007) 12624-12625.
[48] K. Jayasayee, J.A.R.V. Veen, T.G. Manivasagam, S. Celebi, E.J.M. Hensen, F.A. de Bruijn, Appl. Catal. B 111-112 (2012) 515-526.
[49] K. Shinozaki, J.W. Zack, R.M. Richards, B.S. Pivovar, S.S. Kocha, J. Electrochem. Soc. 162 (2015) F1144-F1158.